Neuro-Oncology Advances

6(1), vdae106, 2024 | https://doi.org/10.1093/noajnl/vdae106 | Advance Access date 4 July 2024

Exploring molecular glioblastoma: Insights from advanced imaging for a nuanced understanding of the molecularly defined malignant biology

Michael Griessmair, Claire Delbridge, Julian Ziegenfeuter, Kirsten Jung, Tobias Mueller, Severin Schramm, Denise Bernhardt, Friederike Schmidt-Graf, Olivia Kertels, Marie Thomas, Claus Zimmer, Bernhard Meyer, Stephanie E. Combs, Igor Yakushev, Benedikt Wiestler, and Marie-Christin Metz

All author affiliations are listed at the end of the article

Corresponding Author: Michael Griessmair, MD, Department of Neuroradiology, Klinikum rechts der Isar, TU Munich, Ismaninger Street 22, Munich 81675, Germany (michael.griessmair@tum.de).

Abstract

Background. Molecular glioblastoma (molGB) does not exhibit the histologic hallmarks of a grade 4 glioma but is nevertheless diagnosed as glioblastoma when harboring specific molecular markers. MolGB can easily be mistaken for similar-appearing lower-grade astrocytomas. Here, we investigated how advanced imaging could reflect the underlying tumor biology.

Methods. Clinical and imaging data were collected for 7 molGB grade 4, 9 astrocytomas grade 2, and 12 astrocytomas grade 3. Four neuroradiologists performed VASARI-scoring of conventional imaging, and their inter-reader agreement was assessed using Fleiss κ coefficient. To evaluate the potential of advanced imaging, 2-sample *t* test, 1-way ANOVA, Mann–Whitney U, and Kruskal–Wallis test were performed to test for significant differences between apparent diffusion coefficient (ADC) and relative cerebral blood volume (rCBV) that were extracted fully automatically from the whole tumor volume.

Results. While conventional VASARI imaging features did not allow for reliable differentiation between glioma entities, rCBV was significantly higher in molGB compared to astrocytomas for the 5th and 95th percentile, mean, and median values ($P < .05$). ADC values were significantly lower in molGB than in astrocytomas for mean, median, and the 95th percentile ($P < .05$). Although no molGB showed contrast enhancement initially, we observed enhancement in the short-term follow-up of 1 patient.

Discussion. Quantitative analysis of diffusion and perfusion parameters shows potential in reflecting the malignant tumor biology of molGB. It may increase awareness of molGB in a nonenhancing, "benign" appearing tumor. Our results support the emerging hypothesis that molGB might present glioblastoma captured at an early stage of gliomagenesis.

Key Points

- Conventional imaging fails to properly capture the biological malignancy of molecular glioblastoma.
- Advanced imaging, such as diffusion and perfusion imaging, better reflects the malignant biology of conventionally benign-appearing molGB.
- Molecular glioblastoma might represent glioblastoma detected at an early stage.

Importance of the Study

The 5th edition of the WHO classification for tumors of the central nervous system (CNS) introduced the novel glioma subtype of "molecular glioblastoma" (molGB), which does not exhibit the classical histological and conventional imaging features of a highly malignant grade 4 glioma, and instead is diagnosed by molecular markers alone. Until now, no standardized MRI sequences have been established reflecting this molecularly driven diagnosis. In this pilot study, a unique cohort of 27 similar-appearing gliomas (WHO grades 2–4) was analyzed to demonstrate the value of advanced imaging sequences for revealing tumor biology. MolGB showed significantly higher perfusion and lower diffusion values compared to lower-grade *IDH* mutant astrocytomas, reflecting increased neoangiogenesis and higher cellularity, respectively. Interestingly, observing the natural course of one case, our work also supports the hypothesis that molGB are early-stage glioblastomas that will eventually develop their characteristic appearance, offering a window into early tumor evolution.

The complex interaction of (epi)genetic aberrations for the development and malignant progression of glial tumors has been intensively studied in the past. Thus, a large number of studies demonstrated a highly aggressive course of IDH wild-type gliomas, which exhibit telomerase reverse transcriptase (TERT) promoter mutation, epidermal growth factor receptor (EGFR) amplification, loss of chromosome 10 (whole chromosome, 10p or 10q) or gain of chromosome 7 (whole chromosome, 7p or 7q), even if they do not show the classical histopathological hallmarks of glioblastoma.[1–3] Thus, in the 5th edition of the WHO classification for CNS tumors, the diagnosis of glioblastoma (IDH wild-type WHO CNS grade 4) is possible for the first time only based on the molecular alterations mentioned above.[4] Interestingly, these molecularly defined glioblastoma present not only histologically similar to lower-grade *IDH* mutant astrocytoma, but also on conventional MRI imaging, lacking contrast enhancement and central necrosis. So far, neuroradiology has not been able to detect this molecularly different tumor biology. However, it is likely that these biologically clearly distinct tumor entities also differ in their image phenotype. Few studies investigated differences in tumor localization, initial symptomatology, and signaling behavior on standard MR sequences with no significant findings despite a more diffuse appearance.[5,6]

Interestingly, in a recent work, a small cohort of initially solely molecularly defined glioblastoma (molGB) at recurrence fulfilled the typical morphologic signs of classical glioblastoma on both MR imaging and histology, which made the authors postulate the hypothesis that molGB were simply at an earlier stage of tumorigenesis.[7] This is consistent with the observation that molGB have a similar or slightly greater median overall survival (OS) time than "histological" glioblastoma.[5,8]

In addition, in a recent publication, we demonstrated that molGB already show higher perfusion values in the nonenhancing tumor areas compared to classical glioblastoma (*IDH* wild-type WHO CNS grade 4) or astrocytomas (*IDH* mutant WHO CNS grade 4).[9] One explanation for this could be, for example, that they are at a stage shortly before classical barrier disruption with increased angiogenesis.

Following this observation, in the present study, we aimed to examine possible differences in advanced imaging biomarkers, that is, perfusion and diffusion indices, between molGB and lower-grade astrocytomas, *IDH* mutant. Furthermore, we intended to reassess the aforementioned hypothesis by evaluating the clinical course of the molGB of our cohort. The overall aim of our work was to investigate if advanced imaging could be used to map the malignant tumor biology of MolGB preoperatively and to raise awareness in clinical practice that benign-appearing tumors may harbor highly malignant molecular characteristics.

Methods

Patient Selection

The monocentric retrospective study included a total of 27 patients, who underwent surgery in the period 2020–2022. The patient selection is part of a cohort that has been used for previous work.[9]

Inclusion criteria were preoperative imaging and postoperative neuropathological diagnosis of either IDH wild-type molGB ($n = 7$) (with absence of histological markers of glioblastoma, but occurrence of at least 1 of the following 3 mutations TERT, EGFR amplification, or +7/–10 chromosome) or astrocytomas CNS WHO grade 2 ($n = 9$) or grade 3 ($n = 12$) (harboring IDH mutation) derived from state-of-the-art molecular diagnostics according to the 5th edition of the CNS WHO classification 2021.[4] The clinical course of every patient is provided in Supplementary Table 1.

Because of their usually different appearing in standard MRI, oligodendroglioma were not included in the study. For the quantitative analysis only, all tumors with missing values of diffusion or perfusion imaging and all tumors with border disruption were excluded aiming to find means to differentiate similar-appearing, nonenhancing tumors. All patients signed informed consent for the prospective Glioma registry, which was approved by our local IRB.

Image Analysis

The majority of MR imaging was acquired on a Philips (Best, The Netherlands) 3 Tesla whole-body scanner ($n = 36$) (Achieva or Ingenia) 3 Tesla whole-body scanner. The Philips protocol includes an isotropic FLAIR (voxel size 1 mm^3, echo time (TE) = 269 ms, repetition time (TR) = 4800 ms,

inversion time (TI) = 1650 ms), isotropic T1w turbo field echo (TFE) (voxel size 1 mm^3, TE = 4 ms, TR = 9 ms) before and after contrast, axial T2w (voxel size 0.36 × 0.36 × 4 mm^3, TE = 87 ms, TR = 3396 ms), DSC perfusion (voxel size 1.75 × 1.75 × 4 mm^3, TE = 40 ms, TR = 1547 ms, flip angle = 75°, 80 dynamics), and diffusion tensor imaging (DTI) (TR/TE: 5000/78 ms, voxel size of 2 × 2 × 2 mm^3, 32 diffusion gradient directions, *b* value 1000 s/mm^2)

All available preoperative MRI imaging was evaluated using the same procedure. First, all images were coregistrated into SRI24 Atlas Space using NiftyReg[10,11] and skull-stripped using HD-BET.[12] Fully automated tumor segmentation into necrosis, contrast-enhancing tumor, and edema/noncontrast-enhancing tumor portions was performed using the BraTS Toolkit.[13] As a prerequisite for tumor segmentation, FLAIR, T2, and T1 sequences with (T1-CE) and without administration of contrast agents were required. In case of missing T2 or FLAIR images, a GAN-based approach was performed to synthesize the missing sequence.[14] This was done for 6 patients to enable automated segmentation. Of note, no perfusion or diffusion data were artificially generated.

Advanced imaging modalities (apparent diffusion coefficient, ADC, and cerebral blood volume, CBV) were further postprocessed. Thus, ADC maps were calculated from DTI using dipy.[15] To calculate leakage-corrected CBV, the algorithm of Arzanforoosh et al.[16] was used, which also requires a mask of normal-appearing white matter to normalize the resulting CBV. ANT's Atropos was used for this purpose with the exclusion of tumor areas.[17]

All fully automated tumor segmentations were visually checked for plausibility and Dice Scores have been calculated before to validate agreement with manual tumor delineations.[9] Afterwards, tumor volumes were automatically extracted from the segmentation masks, and summary statistics for ADC and CBV values were collected.

Furthermore, a few visual imaging characteristics from the Visually AcceSAble Rembrandt Images (VASARI) scoring system, namely tumor location (F1), side of tumor epicenter (F2), enhancement quality (F4), and definition of the nonenhancing margin (F13), were listed by 4 neuroradiologists with 2, 2, 3, and 5 years of experience in glioma imaging, respectively (M.G., K.J., T.M., and M.M.).

Positron Emission Tomography Scans

According to a standardized protocol, all O-(2-^{18}F fluoroethyl)-L-tyrosine (FET)–PET scans were performed with a positron emission tomography (PET)/MR scanner (Biograph mMR, Siemens Healthcare GmbH). Four hours before the examination, all patients were instructed to avoid eating. After the target dose of 185 ± 10% MBq 18F-FET was administered, patients were examined after 30–40 minutes. Vendors protocol was used to correct the attenuation.

Neuropathology

After all tissue samples were formalin-fixed and paraffin-embedded, they were diagnosed using the classical neuropathological standard. In addition to conventional histology and immunohistochemistry, an 850k methylation analysis was performed on extracted DNA using Illumina EPIC 850k Methylation Array BeadChip (Illumina Inc.) and evaluated using the Brain Tumor classifier of the DKFZ and the University of Heidelberg.[18,19] This was followed by an integrated diagnosis based on histology, immunohistochemistry, and molecular pathology according to the 5th edition of the WHO classification of 2021.

Statistical Analysis

Patient characteristics, such as age, gender, and initial symptoms at presentation were gathered from the patients' records and analyzed descriptively.

For the VASARI imaging features, inter-reader agreement was assessed using the Fleiss κ coefficient. The κ coefficient was interpreted as follows: 0.20 or less slight agreement, 0.21 to 0.30 fair agreement, 0.41 to 0.60 moderate agreement, 0.61 to 0.80 substantial agreement, and 0.81 to 0.99 almost perfect agreement.

For statistical analysis of the quantitative imaging metrics, that is, voxel-vise ADC values and leakage-corrected CBV values (as stated above), all tumors with contrast enhancement or missing values in perfusion and diffusion imaging were excluded to generate a comparable study group.

Afterwards, in a first step, mean values for ADC and CBV of the whole tumor volume were calculated for 5th percentile, mean, median, and 95th percentile of the molGB on one hand, and astrocytomas CNS grades 2 and 3 together on the other hand. To test for the normality of the sample distribution, Shapiro–Wilk test was performed. For normally distributed parameters, 2-sample *t* test was performed to check for statistically significant differences between the 2 groups. In case of the absence of a normal distribution, Mann–Whitney U test was conducted instead. In both cases, a test for homogeneity of variances was conducted beforehand. Also, 95% confidence intervals were calculated for the mean values, performing bootstrapping in case of non-normally distributed samples. For the differences in medians, a 95% confidence interval was calculated as well.

To further investigate these differences, we separated the 2 different grades of astrocytomas and performed 1-way ANOVA analysis (for normally distributed values) or Kruskal–Wallis test (as the nonparametric alternative) to test for statistically significant differences between the resulting 3 groups (astrocytoma grade 2, astrocytoma grade 3, and molGB). Beforehand, Levene's test for homogeneity of variances was conducted. To see which 2 subgroups differ significantly from each other, Tukey Honestly Significant Difference (HSD) post hoc test was added. Again, 95% confidence intervals were calculated as explained above.

All statistical analyses were done in Python3 using the open-source libraries matplotlib, scipy, seaborn, and statsmodels.

Results

Patient Characteristics

In consideration of the small sample size, a clear difference in the age distribution is already noticeable with a mean age of 56.4 for the molGB group, and 33.1 for astrocytomas CNS grade 2, and 38.1 for astrocytomas CNS grade 3,

respectively. In our cohort, a male predominance in the group of molGB was also visible (see Table 1).

For each patient, the chief symptom at presentation is listed in Table 1. Notably, no symptoms of mass effect, such as headache and nausea, are present in the molGB group. The clinical course of the molGB patients is documented in Supplementary Table 1. Despite adjuvant radiochemotherapy (Stupp protocol), molGB patients showed an average progression-free survival of only 220 days, underlining their biological malignancy.

The distribution of tumor localization as well as presence or absence of contrast enhancement on T1-CE for the 3 groups can be found in Table 1 as well.

For the quantitative analysis, all cases with missing values of diffusion or perfusion imaging and all contrast-enhancing tumors were excluded (as stated in the methods).

That affected $n = 1$ molGB, $n = 2$ astrocytoma WHO CNS grade 2, and $n = 6$ astrocytomas WHO CNS grade 3, which resulted in $n = 6$ molGB, $n = 7$ astrocytomas WHO CNS grade 2, and $n = 6$ astrocytomas WHO CNS grade 3. However, for the sake of completeness, we also performed all analyses using all included gliomas with complete imaging sequences, regardless of the presence or absence of barrier disruption. All results can be found in the supplements.

Differences in Imaging Characteristics and Inter-Reader Agreement

As noted in Table 1, none of our molGB patients showed visible contrast enhancement following gadolinium administration, while it was present in 22% of the patients with astrocytomas WHO CNS grade 2, and in 42% of the patients with astrocytomas WHO CNS grade 3.

The mean κ value for inter-reader agreement for the VASARI features tumor location (F1), side of tumor epicenter (F2), and enhancement quality (F4) was 0.74 (substantial agreement). In contrast, κ coefficient for definition of the nonenhancing margin (F13) was only 0.39, indicating a merely fair agreement between the raters.

Interestingly, all molGB were localized in the temporal lobe and showed no contrast enhancement, as stated above (see Figure 1). In contrast, the localization of astrocytomas was more diverse (refer to Table 1). Notably, one of the molGB showed visibly increased rCBV (see Figure 1A–D), while the other 2 resembled the lower-grade astrocytomas with a not visually observable increased rCBV.

In terms of ADC maps, visual comparison suggests higher ADC values in the tumor regions of the astrocytomas group as opposed to the 3 examples of molGB. In fact, patient 1 even exhibits remarkably decreased ADC values compared to the surrounding white matter (see Figure 1C).

Preoperative [^{18}F] FET-PET Analysis

In addition, 6/7 of the molGB, 9/9 of the astrocytomas (IDH mutant) WHO CNS grade 2, and 8/12 of the astrocytomas (IDH mutant) WHO CNS grade 3 received preoperative FET-PET examination. Thereby, only 2 of the 6 (33%) molGB showed positive PET findings (defined as target

Table 1. Clinical and Imaging Characteristics of Molecular Glioblastoma WHO CNS Grade 4, Astrocytomas WHO ZNS Grade 3, and Astrocytomas WHO ZNS Grade 2

	Molecular glioblastoma CNS WHO grade 4 (*n* = 7; 25%)	Astrocytoma CNS WHO grade 2 (*n* = 9; 32%)	Astrocytoma CNS WHO grade 3 (*n* = 12; 43%)
Age	56.4 ± 4.4	33.1 ± 11.8	38.1 ± 14.9
Sex			
Male	7 (100.0)	4 (44.4)	8 (66.7)
Female	0 (0.0)	5 (55.6)	4 (33.3)
Primary Symptom	Aphasia 3 (42.9)	Seizures 4 (44.4)	Seizures 5 (41.7)
	Personality Changes 1 (14.3)	Incidental 2 (22.2)	Headache 3 (25.0)
	Seizures 1 (14.3)	Unknown 2 (22.2)	Hemiparesis 2 (16.7)
	Fatigue 1 (14.3)	Headache 1 (11.1)	Hemiparesthesia 2 (16.7)
	Memory impairment 1 (14.3)		
Tumor location	Temporal 7 (100.0)	Frontal 4 (44.4)	Temporal 5 (41.7)
		Temporal 4 (44.4)	Frontal 4 (33.3)
		Insular 1 (11.1)	Insular 2 (16.7)
			Brainstem 1 (8.3)
Hemisphere			
Right	1 (14.3)	3 (33.3)	6 (50.0)
Left	6 (85.7)	6 (66.7)	6 (50.0)
Contrast enhancement			
Yes	0 (0.0)	2 (22.2)	5 (41.7)
No	7 (100.0)	7 (77.8)	7 (58.3)

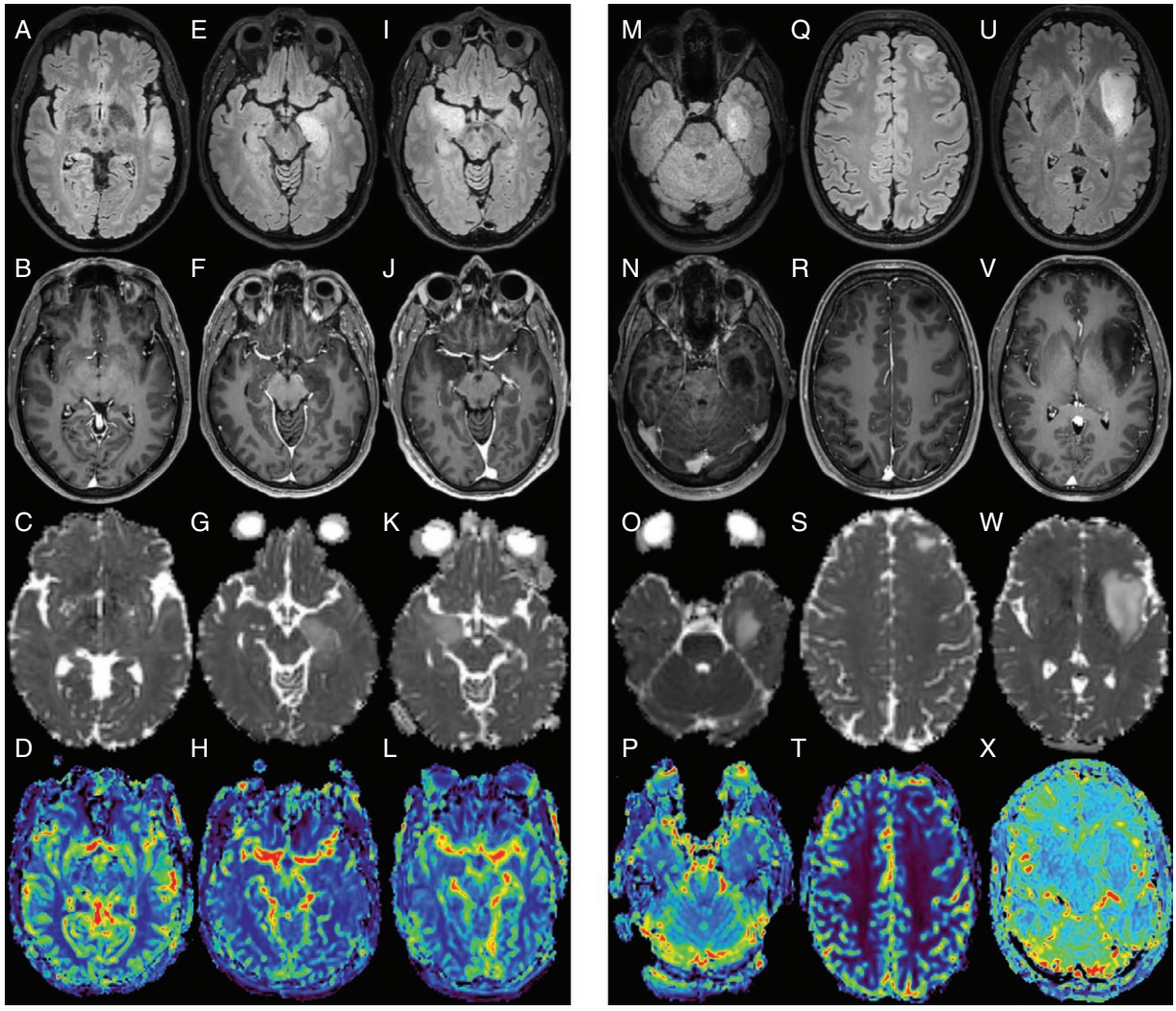

Figure 1. Preoperative MR images of 6 glioma patients, all patients received a complete MRI protocol including T2-FLAIR, T1-CE, ADC, and CBV, preoperatively. On the left side, images of 3 patients with molGB (IDH-wild-type) WHO CNS grade 4 (A–D; E–H; I–L) are depicted on the right side, same sequences are shown for 3 patients with astrocytomas (M–P WHO CNS grade 3; Q–T and U–X WHO CNS grade 2). Depicted sequences are FLAIR (first row), contrast-enhanced T1-weighted images (second row), apparent diffusion coefficient maps (ADC) (third row), and leakage-corrected relative blood volume maps (rCBV) (fourth row). Interestingly, none of the tumors showed extensive contrast enhancement and all tumors despite one molecular glioblastoma (first column C) presented with high ADC values

to background ratio (TBR) > 1.6). Within the group of WHO CNS grade 2 astrocytomas, 6 of the 9 (66%) showed a positive PET finding. In the group of astrocytomas WHO CNS grade 3, 5 of the 8 (63%) showed a positive PET finding.

Quantitative Image Analysis

For quantitative analysis, all tumors with visible contrast enhancement as well as all incomplete advanced imaging sequences were excluded, which resulted in a number of 19 patients. For reference, the results including all acquired 27 glioma patients with complete imaging protocol, regardless of contrast enhancement, can be found in Supplementary Tables.

Mean values for different percentiles, mean, and median of CBV, as well as the results of the 2-sample *t* test or Mann–Whitney U test (for nonnormal distributed samples) between molGB and astrocytomas CNS WHO grade 2 and 3 together, are shown in Supplementary Table 2. Interestingly, molGB exhibited significantly higher rCBV values for 5th percentile ($P = .01$), mean ($P = .01$), and median values ($P = .006$), and for the 95th percentile ($P = .02$), see Figure 2.

In terms of ADC values in the whole tumor volume, molGB demonstrated consequently lower values than the lower-grade astrocytomas, which was statistically significant for the mean ($P = .03$) and median ($P = .02$) and for the 95th percentile of ADC values ($P = .02$), see Figure 2 and Supplementary Table 3.

To further elaborate the differences, we performed 1-way ANOVA or Kruskal–Wallis test (as the nonparametric alternative) to see if the significance of those holds true even when discriminating between astrocytomas WHO CNS grades 2 and 3. Results can be seen in Supplementary Tables 4 and 5.

Surprisingly, rCBV values were higher in astrocytomas WHO CNS grade 2 than in grade 3, although the difference between the 2 groups was not significant in any of the percentiles (as HSD post hoc test revealed). However, differences between all 3 subgroups were significant in the 5th ($P = .02$) and the 95th ($P = .03$) percentile, for mean ($P = .02$), and median ($P = .01$) values (see Supplementary Table 4 and Figure 3).

Similarly, ADC values were lower in astrocytomas WHO CNS grade 2 than in grade 3, except for the 5th percentile. Again, those differences were not significant.

Between the 3 groups, differences in ADC values were significant for the 95th ($P = .03$) percentile (see Supplementary Table 5) with consequently lower ADC values in molGB in all percentiles as reported above (see Figure 3).

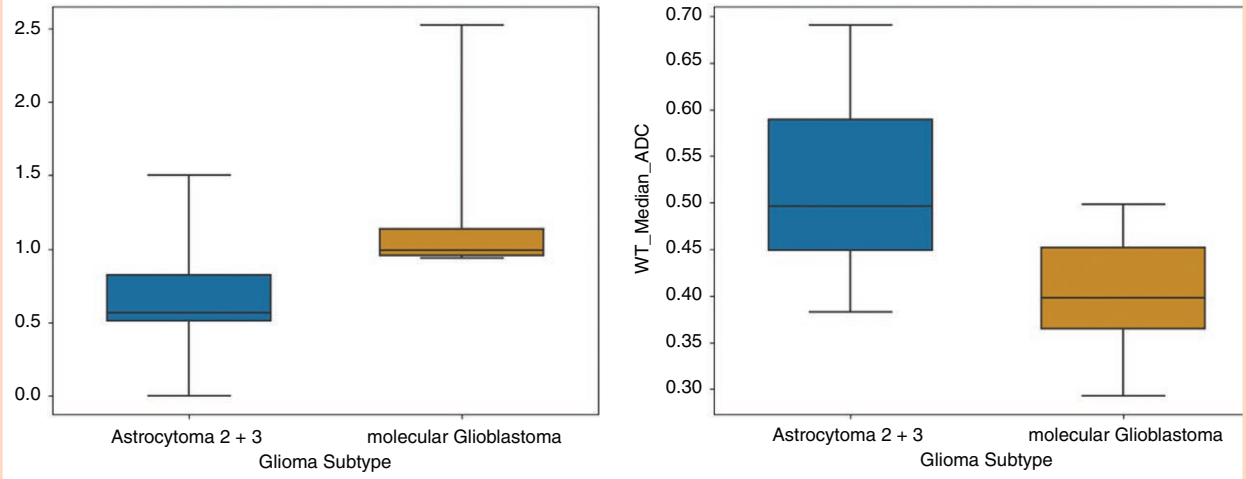

Figure 2. Boxplots illustrating distribution of median values of the whole tumor volume (WT) for relative cerebral blood volume (CBV) (left) and apparent diffusion coefficient (ADC) (right) for molecular glioblastoma ($n = 6$) and astrocytomas WHO CNS grade 2 + 3 ($n = 13$): molecular glioblastoma showed significant higher CBV ($P = .01$) and lower ADC values ($P = .02$) compared to lower-grade astrocytomas.

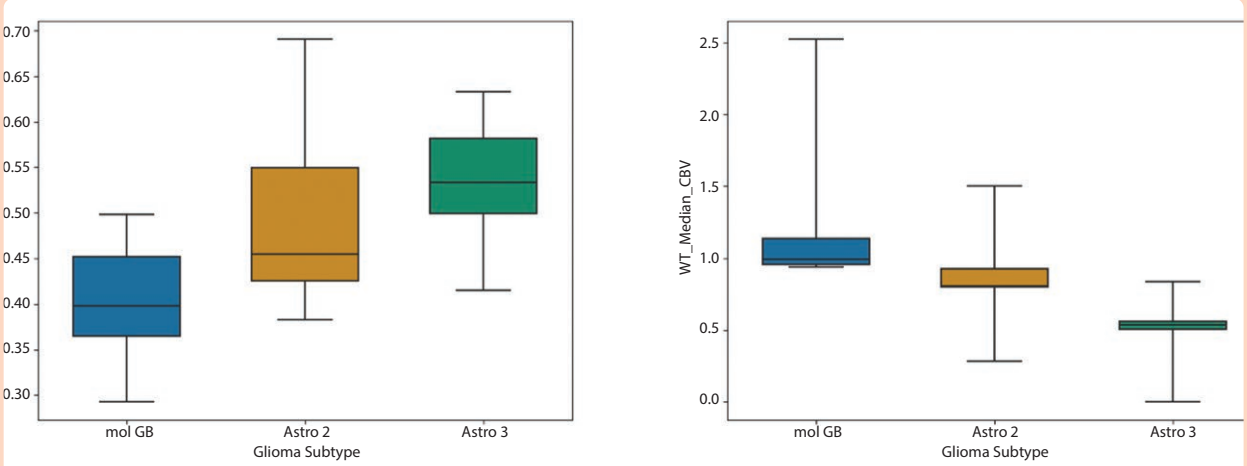

Figure 3. Comparison of WT (whole tumor) median relative cerebral blood volume (CBV) values and median apparent diffusion coefficient (ADC) values of molecular glioblastoma (molGB), WHO CNS grade 4 ($n = 6$), Astro2 (astrocytomas WHO CNS grade 2 [IDH mutant, not 1p/19q codeleted]) ($n = 7$), Astro3 (astrocytomas WHO CNS grade 3 [IDH mutant, not 1p/19q codeleted]) ($n = 6$). MolGB showed higher CBV compared to both of the astrocytoma subgroups. On a side note, astrocytomas WHO CNS grade 2 demonstrated higher CBV compared to astrocytomas WHO CNS grade 3. Interestingly, molGB showed lower ADC values compared to astrocytomas. Between the two astrocytoma grades, there were noticeable differences as well.

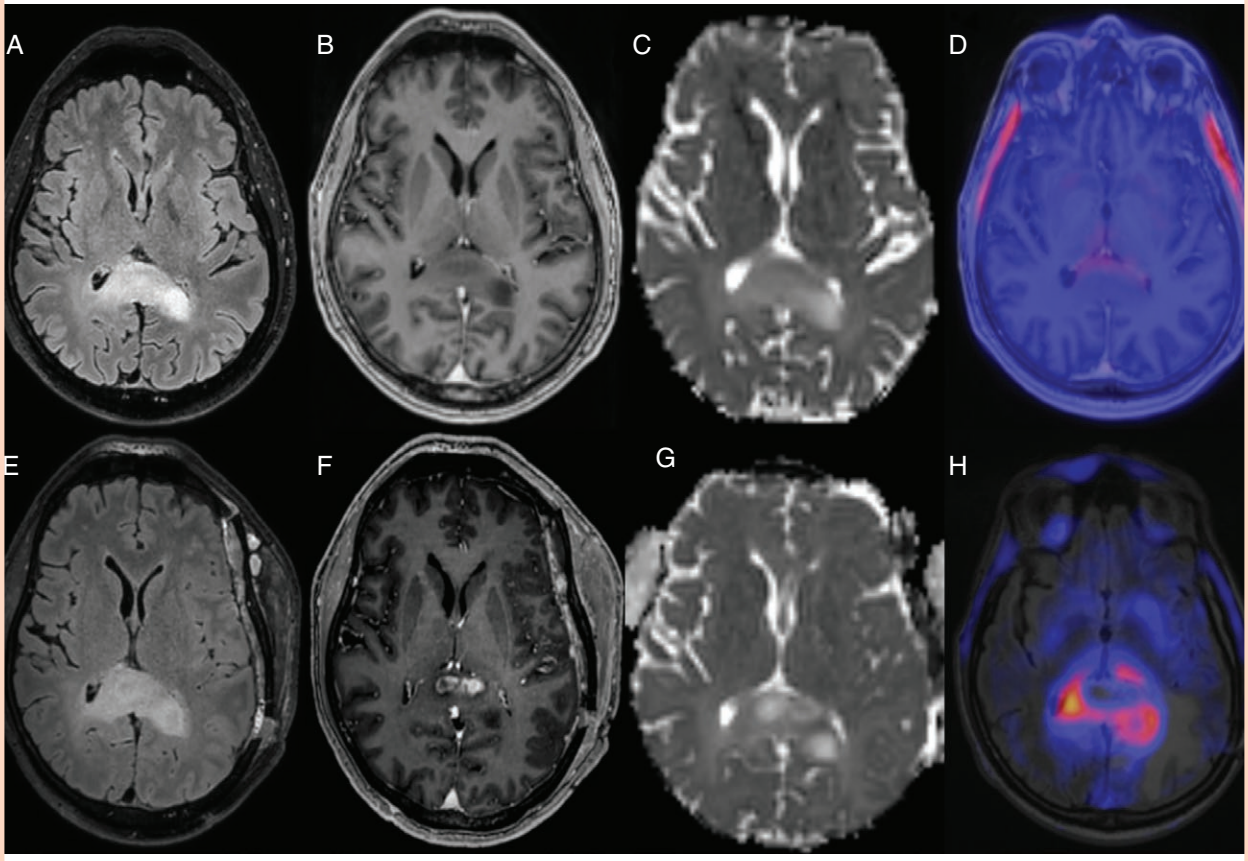

Figure 4. Presents a patient with preoperative MRI imaging/PET scan (A–D) and with postoperative MRI imaging/PET scan 30 days later (E–H). The tumor portion shown was not resected. In addition, no adjuvant therapy was performed. Depicted sequences are FLAIR (first row), contrast-enhanced T1-weighted images (second row), apparent diffusion coefficient maps (ADC, third row), and PET scan (fourth row). Interestingly, PET was negative in the beginning and got positive in progression.

Single Case Study With Natural Course of a "Molecular Glioblastoma"

The course in Figure 4 shows a patient who presented clinically with progressive disorientation and short-term memory impairment. MRI imaging revealed a FLAIR-hyperintense left temporal mass extending into the splenium of the corpus callosum without barrier disruption, leading to a radiological diagnosis of low-grade glioma. Surgically, only the rostral parts of the tumor in the temporal lobe were removed (not depicted). Neuropathological analysis showed no necrosis or vascular proliferation (see Figure 5), but 850K methylation analysis revealed IDH wild-type status and EGFR amplification, loss of chromosome 10 and gain of chromosome 7. TERT promoter mutation was not evaluated. Based on these findings, a diagnosis of glioblastoma (IDH wild-type) was made according to the 5th edition of the WHO CNS 2021 classification. In the second postoperative MRI control, 30 days after the initial MR examination, the nonresected tumor parts in the splenium of the corpus callosum showed a barrier disruption with central necrotic parts. It should be mentioned that no radiochemotherapy was performed in the meantime, which excludes the possibility of contrast enhancement due to radiation necrosis. A PET scan was also performed both preoperatively and in progressive disease. Initially, a TBR mean of 1.4 (norm < 1.6) was found; therefore, a higher-grade glial tumor was rather excluded. Interestingly, with the onset of the barrier disorder, PET was also positive with a TBR mean of 2.3 (norm after radiotherapy < 2.0). It should be mentioned that the patient received radiotherapy before the PET examination. This case illustrates an example for the "natural" radiological course of a molGB.

Discussion

The objective of our work was to investigate the added value of quantitative analysis of advanced imaging, including perfusion and diffusion imaging, for revealing the malignant tumor biology of molGB, which is defined on a molecular basis. Although it should not be regarded as a differentiation tool, it offers a future possibility in the preoperative differentiation from similar-appearing lower-grade astrocytoma (IDH mutant) WHO grade 2 or 3. Astrocytomas WHO grade 4 were not included because differences in advanced imaging parameters to molGB have

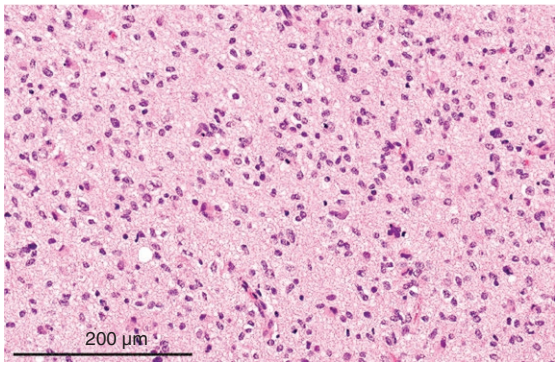

Figure 5. HE staining of postoperative tissue shows an infiltrating glial tumor with high cell density without necrosis and vessel proliferation. Subsequent molecular analysis revealed a diagnosis of glioblastoma WHO CNS grade 4.

already been highlighted in a previous work.[9] For this purpose, 27 glioma patients were included in the study and examined for differences in patient characteristics and visual imaging features, including selected VASARI features and quantitative imaging markers of diffusion and perfusion imaging.

As reported in previous work, our molGB were strictly temporally located and showed no contrast enhancement.[6,20–22] On standard MR sequences, tumor boundaries of molGB appeared to be more infiltrative in comparison to the more defined boundaries of the IDH mutant astrocytomas as described in the literature.[22,23] However, this observation did not receive a high inter-reader agreement, which could be explained by the necessity of advanced experience in glioma imaging, which not all readers held equally. Also, the age distribution of molGB patients (mean age 56.4 years) as well as the predominance of male gender are in accordance with prior studies.[8,24] In contrast, the astrocytomas studied (IDH mutant) were diverse in distribution, younger in age (mean age 33.1 for astrocytomas WHO CNS grade 2 and mean age 38.1 for astrocytomas WHO CNS grade 3), and showed some tendency toward the frontal lobe, which has been linked to IDH mutation status in a recent systematic meta-analysis.[25] Interestingly, differentiation of molGB and astrocytomas WHO CNS grade 2/3 based on the initial clinical presentation was not possible. MolGB were often diagnosed following symptoms like speech disturbances or epileptic seizures and did not cause symptoms of mass effect such as headache and nausea. Thus, the clinical appearance is more similar to that of low-grade gliomas than to "classical" glioblastoma.[26] Furthermore, even by FET-PET examination, differentiation between the entities was not possible in our cohort. In fact, molGB were less frequently PET positive than low-grade astrocytomas. No relevant data currently exist regarding PET studies in molGB. Further analysis would be of great interest here.

For the quantitative analysis of perfusion and diffusion parameters, all contrast-enhancing tumors were excluded (and all cases with missing values of diffusion or perfusion imaging) to guarantee similarity between the subgroups.

In fact, molecularly defined glioblastoma showed significantly higher values of mean rCBV in the whole tumor volume compared to lower-grade astrocytoma, IDH mutant, and significantly lower mean values of ADC, which might be indicative of higher cellularity.[27]

These findings might have a significant impact on the differentiation of those entities in the future. This differentiation is clinically highly important since molGB have (due to their "benign" appearance) often been misdiagnosed as lower-grade gliomas in the past, which did not only delay appropriate treatment but also caused additional stress on the patient, who had to receive a much worse, revised diagnosis and prognosis after the histopathologic results. However, confirmation of the data on a larger cohort is definitely necessary.

Looking at the increased rCBV in molGB, we hypothesize that those are observed in a time frame of tumorigenesis, where blood flow increases due to the elevation of angiogenic factors such as VEGF (vascular endothelial growth factor), but full disruption of the blood–brain barrier that allows leakage of macromolecules such as gadolinium has not yet occurred.[28–30] Further, research has shown that IDH mutations are associated with lower VEGF expressions, which may be another reason for the lower rCBV values in these entities.[31]

Interestingly, for one case of our molGB patients, we could observe some kind of natural course of this tumor, which developed contrast enhancement in the primary nonenhancing tumor portions after 30 days without adjuvant treatment. This case might also support the already postulated hypothesis of molGB being early detected, "classic" glioblastoma that often appear as classical histologic glioblastoma when recurring.[7] However, it remains unclear why patients suffering from molGB become symptomatic at an earlier stage and why the tumors occur mostly in the temporal lobe. One possible reason for the clustered occurrence in the temporal lobe may be the theory that gliomas arise by malignant transformation from stem cells derived from the subventricular zone.[32] Thus, mutations were identified in neural stem cells of the subventricular zone, which are considered to function as driver mutations in glioblastoma.[33,34] Additionally, radiation of the ipsilateral subventricular zone after resection leads to longer progression-free survival but no significant change in OS,[35] which also supports this hypothesis. On a side note, astrocytomas (IDH mutant) WHO CNS grade 2 showed higher perfusion values than astrocytomas (IDH mutant) WHO CNS grade 3, albeit not on a significant level. This might be due to the fact that we excluded all contrast-enhancing tumors in this analysis, and that grade 2 astrocytomas, in contrast to grade 3 astrocytomas, more rarely exhibit edema, and therefore, the nonenhancing mass mostly reflects tumor tissue.[36] In addition, it could also simply be caused by a sampling error.

Ultimately, evidence rises that biological behavior between molecular and histologic glioblastoma still differs substantially with longer progression-free survival, longer median OS for molGB,[8,24] and missing survival benefit from temozolomide for this subgroup, regardless of MGMT promotor methylation status.[37]

Therefore, more research needs to be done to fully comprehend this novel sub-entity of glioblastoma.

Limitations

While our work provides interesting insights into the imaging aspects of the biology of gliomas, some limitations exist. Although the detailed sequences and methylation analyses of the included tumors are remarkable, the cohort ($n = 27$) is relatively small, which, however, is also due to the lower prevalence of the included tumors. This also limits the immediate clinical applicability. On the other hand, our results warrant larger studies specifically looking into the role of advanced imaging to aid the preoperative differentiation of these tumors.

In addition, this is a single-center study only, which in turn enables a more standardized neuroradiological and pathological diagnostic process. We encourage further research on this topic to test the generalizability of our results on different scanners and larger patient cohorts.

Conclusion

This study demonstrates the potential of quantitative diffusion and perfusion imaging for characterizing the highly malignant biology of molGB compared to conventional imaging techniques. By revealing significantly higher perfusion and lower ADC values in molGB compared to *IDH* mutant lower-grade gliomas, these approaches provide objective measures of increased neoangiogenesis and cellularity, hallmarks of aggressive tumors.

Beyond characterization, our findings suggest that these imaging techniques could offer a noninvasive window into the early malignant progression of molGB. This deeper understanding potentially paves the way for earlier detection and intervention, improving patient outcomes.

Future multicentric studies are warranted to validate these promising results. Such investigations should explore the role of quantitative diffusion and perfusion imaging in preoperative differentiation and noninvasive assessment of tumor evolution across diverse patient populations.

Supplementary material

Supplementary material is available online at *Neuro-Oncology Advances* (https://academic.oup.com/noa).

Keywords

850k methylation analysis | advanced imaging biomarkers | fully automated tumor segmentations | tumorigenesis of glioblastoma

Funding

None declared.

Conflict of interest statement

None declared.

Authorship statement

Conceptualization, B.W., M.M., and M.G.; methodology, C.D. and B.W.; software, B.W. and M.T.; validation, J.G., H.M., B.M., Y.Y., and I.Y.; formal analysis, B.W. and M.M.; resources, C.D., J.G., H.M., B.M., I.Y., F.S.G., C.Z., D.B., and S.C.; data curation, M.G., J.Z., O.K., and M.M.; writing—original draft preparation, M.G. and M.M.; writing—review and editing, C.D. and B.W.; visualization, M.M., and M.G.; supervision, B.W. and M.M.; project administration, B.W.

Affiliations

Department of Neuroradiology, Klinikum Rechts der Isar, TU Munich, Munich, Germany (M.G., J.Z., K.J., T.M., S.S., O.K., M.T., C.Z., B.W., M.-C.M.); Department of Pathology, TU Munich, Munich, Germany (C.D.); Department of Radiation Oncology, Klinikum Rechts der Isar, TU Munich, Munich, Germany (D.B., S.E.C.); Department of Neurosurgery, Klinikum Rechts der Isar, TU Munich, Munich, Germany (B.M.); Department of Neurology, Klinikum Rechts der Isar, TU Munich, Munich, Germany (F.S.-G.); Department of Nuclear Medicine, Klinikum Rechts der Isar, TU Munich, Munich, Germany (I.Y.); TranslaTUM, TU Munich, Munich, Germany (B.W.)

References

1. Weller M, Weber RG, Willscher E, et al. Molecular classification of diffuse cerebral WHO grade II/III gliomas using genome- and transcriptome-wide profiling improves stratification of prognostically distinct patient groups. *Acta Neuropathol (Berl).* 2015;129(5):679–693.
2. Wijnenga MMJ, Dubbink HJ, French PJ, et al. Molecular and clinical heterogeneity of adult diffuse low-grade IDH wild-type gliomas: assessment of TERT promoter mutation and chromosome 7 and 10 copy number status allows superior prognostic stratification. *Acta Neuropathol (Berl).* 2017;134(6):957–959.
3. Eckel-Passow JE, Lachance DH, Molinaro AM, et al. Glioma groups based on 1p/19q, IDH, and TERT promoter mutations in tumors. *N Engl J Med.* 2015;372(26):2499–2508.
4. Louis DN, Perry A, Wesseling P, et al. The 2021 WHO classification of tumors of the central nervous system: a summary. *Neuro Oncol.* 2021;23(8):1231–1251.
5. Grogan D, Bray DP, Cosgrove M, et al. Clinical and radiographic characteristics of diffuse astrocytic glioma, IDH-wildtype, with molecular features of glioblastoma: a single institution review. *J Neurooncol.* 2022;157(1):187–195.
6. Lee D, Riestenberg RA, Haskell-Mendoza A, Bloch O. Diffuse astrocytic glioma, IDH-wildtype, with molecular features of glioblastoma, WHO

grade IV: a single-institution case series and review. *J Neurooncol.* 2021;152(1):89–98.
7. Ramos-Fresnedo A, Domingo RA, Perez-Vega C, et al. The early infiltrative phase of GBM hypothesis: are molecular glioblastomas histological glioblastomas in the making? A preliminary multicenter study. *J Neurooncol.* 2022;158(3):497–506.
8. Ramos-Fresnedo A, Pullen MW, Perez-Vega C, et al. The survival outcomes of molecular glioblastoma IDH-wildtype: a multicenter study. *J Neurooncol.* 2022;157(1):177–185.
9. Griessmair M, Delbridge C, Ziegenfeuter J, et al. Imaging the WHO 2021 brain tumor classification: fully automated analysis of imaging features of newly diagnosed gliomas. *Cancers (Basel).* 2023;15(8):2355. doi:10.3390/cancers15082355
10. Modat M, Cash DM, Daga P, et al. Global image registration using a symmetric block-matching approach. *J Med Imaging.* 2014;1(2):024003.
11. Rohlfing T, Zahr NM, Sullivan EV, Pfefferbaum A. The SRI24 multichannel atlas of normal adult human brain structure. *Hum Brain Mapp.* 2010;31(5):798–819.
12. Isensee F, Schell M, Pflueger I, et al. Automated brain extraction of multisequence MRI using artificial neural networks. *Hum Brain Mapp.* 2019;40(17):4952–4964.
13. Kofler F, Berger C, Waldmannstetter D, et al. BraTS toolkit: translating brats brain tumor segmentation algorithms into clinical and scientific practice. *Front Neurosci.* 2020;14(125):125.
14. Thomas MF, Kofler F, Grundl L, et al. Improving automated glioma segmentation in routine clinical use through artificial intelligence-based replacement of missing sequences with synthetic magnetic resonance imaging scans. *Invest Radiol.* 2022;57(3):187–193.
15. Garyfallidis E, et al. Dipy, a library for the analysis of diffusion MRI data. *Front Neuroinformatics.* 2014;8(8).
16. Arzanforoosh F, Croal PL, van Garderen KA, et al. Effect of applying leakage correction on rCBV measurement derived from DSC-MRI in enhancing and nonenhancing glioma. *Front Oncol.* 2021;11(648528):648528.
17. Avants BB, Tustison NJ, Wu J, Cook PA, Gee JC. An open source multivariate framework for n-tissue segmentation with evaluation on public data. *Neuroinformatics.* 2011;9(4):381–400.
18. Capper D, Jones DTW, Sill M, et al. DNA methylation-based classification of central nervous system tumours. *Nature.* 2018;555(7697):469–474.
19. Capper D, Stichel D, Sahm F, et al. Practical implementation of DNA methylation and copy-number-based CNS tumor diagnostics: the Heidelberg experience. *Acta Neuropathol (Berl).* 2018;136(2):181–210.
20. Metellus P, Coulibaly B, Colin C, et al. Absence of IDH mutation identifies a novel radiologic and molecular subtype of WHO grade II gliomas with dismal prognosis. *Acta Neuropathol (Berl).* 2010;120(8):719–729.
21. Izquierdo C, Barritault M, Poncet D, et al. Radiological characteristics and natural history of adult IDH-wildtype astrocytomas with TERT promoter mutations. *Neurosurgery.* 2019;85(3):E448–E456.
22. Darlix A, Deverdun J, Menjot de Champfleur N, et al. IDH mutation and 1p19q codeletion distinguish two radiological patterns of diffuse low-grade gliomas. *J Neurooncol.* 2017;133(1):37–45.
23. van Lent DI, van Baarsen KM, Snijders TJ, Robe PAJT. Radiological differences between subtypes of WHO 2016 grade II-III gliomas: a systematic review and meta-analysis. *Neurooncol Adv.* 2020;2(1):vdaa044.
24. Berzero G, Di Stefano AL, Ronchi S, et al. IDH-wildtype lower-grade diffuse gliomas: the importance of histological grade and molecular assessment for prognostic stratification. *Neuro Oncol.* 2021;23(6):955–966.
25. Lasocki A, Anjari M, Örs Kokurcan S, Thust SC. Conventional MRI features of adult diffuse glioma molecular subtypes: a systematic review. *Neuroradiol.* 2021;63(3):353–362. https://link-springer-com.eaccess.tum.edu/article/10.1007/s00234-020-02532-7
26. van Opijnen MP, Tesileanu CMS, Dirven L, et al. IDH1/2 wildtype gliomas grade 2 and 3 with molecular glioblastoma-like profile have a distinct course of epilepsy compared to IDH1/2 wildtype glioblastomas. *Neuro Oncol.* 2023;25(4):701–709.
27. Eidel O, Neumann J-O, Burth S, et al. Automatic analysis of cellularity in glioblastoma and correlation with ADC using trajectory analysis and automatic nuclei counting. *PLoS One.* 2016;11(6):e0160250.
28. Arvanitis CD, Ferraro GB, Jain RK. The blood-brain barrier and blood-tumour barrier in brain tumours and metastases. *Nat Rev Cancer.* 2020;20(1):26–41.
29. Luo H, Shusta EV. Blood-brain barrier modulation to improve glioma drug delivery. *Pharmaceutics.* 2020;12(11):1085.
30. Hardee ME, Zagzag D. Mechanisms of glioma-associated neovascularization. *Am J Pathol.* 2012;181(4):1126–1141.
31. Polívka J, Pešta M, Pitule P, et al. IDH1 mutation is associated with lower expression of VEGF but not microvessel formation in glioblastoma multiforme. *Oncotarget.* 2018;9(23):16462–16476.
32. Altmann C, Keller S, Schmidt MHH. The role of SVZ stem cells in glioblastoma. *Cancers.* 2019;11(4):448.
33. Brennan CW, Verhaak RGW, McKenna A, et al.; TCGA Research Network. The somatic genomic landscape of glioblastoma. *Cell.* 2013;155(2):462–477.
34. Beiriger J, Habib A, Jovanovich N, et al. The subventricular zone in glioblastoma: genesis, maintenance, and modeling. *Front Oncol.* 2022;12(790976):790976.
35. Şuşman S, Leucuţa D-C, Kacso G, Florian I. High dose vs low dose irradiation of the subventricular zone in patients with glioblastoma—a systematic review and meta-analysis. *Cancer Manag Res.* 2019;11:6741–6753.
36. Wang W, Da R, Wang M, et al. Expression of brain-specific angiogenesis inhibitor 1 is inversely correlated with pathological grade, angiogenesis and peritumoral brain edema in human astrocytomas. *Oncol Lett.* 2013;5(5):1513–1518.
37. Tesileanu CMS, Sanson M, Wick W, et al. Temozolomide and radiotherapy versus radiotherapy alone in patients with glioblastoma, IDH-wildtype: post hoc analysis of the EORTC Randomized Phase III CATNON Trial. *Clin Can Res.* 2022;28(12):2527–2535.